

# Graph Layer Security: Encrypting Information via Common Networked Physics

Zhuangkun Wei<sup>1</sup>, Schyler C. Sun<sup>3</sup>, Bin Li<sup>4</sup>, Weisi Guo<sup>1,2,3\*</sup>

**Abstract**—The proliferation of low-cost Internet of Things (IoT) devices has led to a race between wireless security and channel attacks. Traditional cryptography requires high-computational power and is not suitable for low-power IoT scenarios. Whilst, recently developed physical layer security (PLS) can exploit common wireless channel state information (CSI), its sensitivity to channel estimation makes them vulnerable from attacks. In this work, we exploit an alternative common physics shared between IoT transceivers: the monitored channel-irrelevant physical networked dynamics (e.g., water/oil/gas/electrical signal-flows). Leveraging this, we propose for the first time, graph layer security (GLS), by exploiting the dependency in physical dynamics among network nodes for information encryption and decryption. A graph Fourier transform (GFT) operator is used to characterize such dependency into a graph-bandlimited subspace, which allows the generations of channel-irrelevant cipher keys by maximizing the secrecy rate. We evaluate our GLS against designed active and passive attackers, using IEEE 39-Bus system. Results demonstrate that, GLS is not reliant on wireless CSI, and can combat attackers that have partial networked dynamic knowledge (realistic access to full dynamic and critical nodes remains challenging). We believe this novel GLS has widespread applicability in secure health monitoring and for Digital Twins in adversarial radio environments.

**Index Terms**—cyber-physical systems, wireless security, sensor network, infrastructure health monitoring, graph signal processing

## I. INTRODUCTION

Mass digitization of people and things has opened the doorway to the Internet of Things (IoT), critical in many social and industrial applications [1], [2]. In particular, IoT is envisaged to deliver the vital data to inform Digital Twins and improve infrastructure maintenance and safety. In many cases, wireless IoT sensors that measure physical signals (e.g. gas pressure, water contamination) are buried underground [3], [4]. Encrypting the critical infrastructure information is important for national security, commercial sensitivity, and anti-tampering requirements. Many current IoT wireless transmissions (e.g. LoRaWAN [5], ZigBee) are vulnerable to eavesdropping. Authentication (e.g. over-the-air activation session keys in LoRaWAN, Elliptic Curve Diffie-Hellman in Bluetooth) verifies the user's identity and prevents malicious users from accessing the network. Encrypted wireless transmission protects data integrity and confidentiality [6].

## A. From Public Key Cryptography to Physical Layer Security

Conventional encrypted communications employ symmetric encryption such as the advanced encryption standard (AES), which relies on a secret key shared between them beforehand. Public key cryptography (PKC) is the de facto key distribution protocol. Although efficient conventional PKC schemes are complex and computationally not suitable for IoT devices with limited capability [7]. This introduces not only a computational cost challenge, but also sets the IoT devices at a disadvantage against most powerful eavesdroppers with orders of magnitude more computational power.

Physical layer security (PLS) has been proposed in recent years as a way to overcome many of the aforementioned challenges by exploiting the randomness and the superiority of the legitimate wireless channel over wiretap channel properties without the need for a PKC distribution protocol [6], [8], [9]. PLS negates the risk of key intercept and high computational requirement of PKC schemes, which makes it very suitable for IoT devices. PLS does however require that the wireless channel between nodes to be reciprocal (true for most propagation environments), dynamic (fading), and unique [10], [11]. This is to ensure robust symmetric key generation and avoid brute force attempts. PLS has been applied to a variety of embedded wireless and wired communication systems [12]–[17]. The shortfall of PLS lies in it requires the IoT devices to make accurate estimations of the wireless channel statistics [18]. Accurate estimation requires reasonably powerful signal processing units and also requires a reasonably high communication signal to noise ratio (SNR). Many embedded or underground IoT devices operate in low communication SNR regimes, and therefore PLS is not suitable.

## B. Introducing Graph Layer Security (GLS): Encryption using Networked Physics

To overcome the PLS requirement of a high communication SNR for accurate wireless channel estimation, we identify and exploit a different physical attribute that is common to many IoT sensors. The general idea to exploit common physics has been proposed before, such as common heartbeat in different medical IoT devices across a body. However, those devices typically do not suffer from the aforementioned low communication SNR challenges. Here, we consider IoT devices placed in underground or embedded networked systems, such as oil/gas/water pipes, electrical networks, optical fibre networks, and other underground connected systems. In networked physical systems, a common continuity equation connects all the dynamics (e.g. Navier Stokes for flow, Nonlinear Schrodinger

<sup>1</sup>University of Warwick, UK. <sup>2</sup>The Alan Turing Institute, UK. <sup>3</sup>Cranfield University, UK. <sup>4</sup>Beijing University of Posts and Telecommunications, China. \*Corresponding Author: weisi.guo@cranfield.ac.uk.

for optic transmission, power flow for electricity). We propose to exploit the common networked physical signals at different IoT monitoring points to encrypt the IoT device's wireless data. This has the advantage of: 1) IoT sensors usually have very high precision in measuring the physical signals, and 2) requires no specific knowledge or requirement of wireless channel or public key distribution. This novel physical driven security is distinctive from both PKC and PLS, and its security independence from the digital environment makes it more resilient against digital attacks. The main contributions of this work are summarized in the following.

(1) We propose a novel digital encryption paradigm over a physical network - called graph layer security (GLS). The process is **data driven** and **model agnostic**. We exploit the dependency of underlying networked physical dynamics to enable encryption amongst digital transceivers, without complex computations (for key generation/management in traditional cryptography-based method, or for channel estimating techniques in PLS). In GLS, the encryption and decryption is based on an additive noise generated by the wireless channel-irrelevant physical networked dynamic on one node, and can be compensated by other nodes with dependent networked dynamics. Leveraging this idea, for any pair of network nodes as Tx and Rx, we select the relay nodes with dependent dynamics, and the information then can be encrypted, reconciliated, and finally decrypted by Tx, relay and Rx nodes.

(2) One difficulty of the relay selection lies in the dependency analysis on the random networked dynamics. To overcome this, we draw heavily on sparsifying high dimensional random nonlinear dynamics by the use of a data-driven Graph Fourier Transform (GFT) operator, which is able to transform the random dynamics into a compact graph bandlimited subspace, given the graph smoothness of the evolved networked dynamics (or its time-difference) [19]. By doing so, we pursue the dependency analysis of the random dynamics by finding the dependent rows of the GFT based surrogate matrix.

(3) We analyze and evaluate the performance of our proposed GLS, using IEEE 39-Bus system. Both the passive eavesdroppers and the active attackers are considered, where the former is defined as intercepting the transmitted information (encrypted) as well as hacking parts of the network nodes and their dynamics, and the latter is defined to degrade the dynamic dependency by adding jamming perturbations to the network. The simulations show two results. First, the GLS performance depends mostly on the measuring accuracy of the networked dynamics, other than the complex channel estimation techniques for key generations required by the PLS. Second, GLS can protect communication security from the eavesdroppers; the bit error rate (BER) of the legitimate (Tx,Rx) pair can approach an order of  $10^{-5}$  as opposed to the passive eavesdroppers ( $10^{-1}$ ), and can still remain an order of  $10^{-3}$  in the face of active dynamic attacker. This suggests a promising prospect of the proposed GLS to secure the wireless communications using the graph layer common physics.

The rest of the paper is organised as follows. In Section II, we introduce the network dynamic model, including governing evolution pattern that maintains the dynamic dependency, and

the perturbation to keep the randomness of the networked dynamics. In Section III, we elaborate the GLS encryption and decryption process, as well as how to select the relays for each (Tx,Rx) pair. Also, we define the passive eavesdroppers and active attackers and analyze their influences on the GLS performance. The simulation results are provided in Section IV. We finally conclude the whole piece of work in Section V.

## II. PHYSICAL DYNAMIC MODEL FOR DATA ENCRYPTION

In this section, we introduce the physical networked dynamic model for further encryption of wireless communications. The networked dynamic is described by the underlying network topology and the dynamic signal flow over it. The network topology is configured by a static graph, denoted by  $\mathcal{G}(\mathcal{N}, \mathbf{W})$ . Here,  $\mathcal{N} = \{1, \dots, N\}$  represents a set of total node indices.  $\mathbf{W}$  of size  $N \times N$  is the adjacent matrix, in which the  $(m, n)$ th element  $w_{m,n} \in \{0, 1\}$  reflects the existence of directed link from node  $n$  to  $m$ .

Given the topology of the network, the dynamic signal over each node evolves in accordance with its self-dynamic and the coupling interactions from its neighbouring (connected) nodes. We denote the signals for all  $k = 1, \dots, K$  ( $K \in \mathbb{N}^+$ ) discrete time as a matrix  $\mathbf{X}$  of size  $N \times K$ , and the evolution function from discrete time  $k$  to  $k + 1$  as  $\mathbf{F} : \mathbb{R}^N \rightarrow \mathbb{R}^N$ . Then, the networked dynamic model is expressed as:

$$\mathbf{X}_{:,k+1} = \mathbf{F}(\mathbf{X}_{:,k}) + \mathbf{b}_k, \quad (1)$$

where  $\mathbf{X}_{:,k}$  represents the  $k$ th column of  $\mathbf{X}$ .

In Eq. (1),  $\mathbf{b}_k$  is the perturbations that account for the randomness of the dynamic. We specify  $\mathbf{b}_k$  by the compositions of the unknown injection amplitude  $\mathbf{b}_{k_i}$  of size  $N \times 1$  with respect to a random injection-time (i.e.,  $k_i$ ), governed by the Dirac delta function, i.e.,

$$\mathbf{b}_k = \sum_{k_i \in \mathbb{N}^+} \mathbf{b}_{k_i} \cdot \delta(k - k_i). \quad (2)$$

In Eq. (2), both the injection amplitudes and time are unknown, and may have different distributions for different dynamic systems. For this work, we do not rely on the exact distribution of the perturbations, but assume its sparse appearance (e.g., the contaminant injection into a water-distribution network, or the steep variations of the power-usages in an electrical bus system are sparse). As such, the combination of the networked evolution model  $\mathbf{F}(\cdot)$  and the random perturbation will provide the dynamic dependency as well as the randomness to secure the dynamic-irrelevant wireless communications, and is hard to be guessed by brute force, unless the total underlying network dynamics are hacked. We will then elaborate how to pursue information encryption and decryption using the graph layer dynamics.

## III. GLS ENCRYPTION USING PHYSICAL NETWORKED DYNAMIC

Given the modelling of Eqs. (1)-(2), the purpose of this work is to encrypt the wireless communications of any node pair, using the underlying physical dynamics of the graph layer. The illustration of the GLS is provided by Fig. 1. For any node

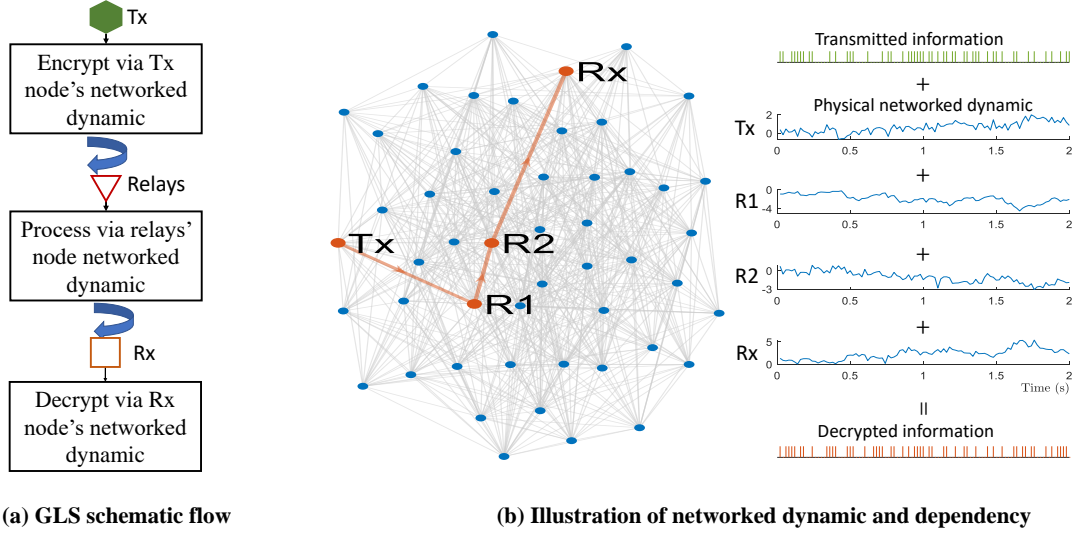


Fig. 1. Illustration of graph layer security, where the wireless communications between  $(Tx, Rx)$  node pair is secured by the wireless channel -irrelevant physical networked dynamics. The encryption and decoding are leveraging the linear dependency of networked dynamics. (a) shows the GLS schematic flow. (b) presents the illustration of the physical networked dynamic and the linear dependency among  $(Tx, Relays, Rx)$ .

$n$  to act as the Tx, we encrypt the desirable information  $s$  (a time-series of length  $L$ ) via the physical networked dynamic on node  $n$ , denoted as  $\mathbf{X}_{n,:}$ , i.e.,

$$\mathbf{s}^* = \mathbf{s} + \mathbf{X}_{n,:}, \quad (3)$$

where  $\mathbf{s}^*$  is the encrypted information to be transmitted.

After the information encryption using Eq. (3) at Tx node, it will then be transmitted and processed via a group of selected relays and their dynamics (e.g., R1 and R2 in Fig. 1(b)). At the final Rx node, the encrypted information will be received and decrypted. As such, for the wireless communication between any node pair, i.e.,  $(Tx, Rx) = (n, m)$ , the idea of encryption and encryption is leveraging the linear dependency of the underlying physical dynamics in Tx, relays, and Rx nodes, i.e.,

$$\mathbf{X}_{n,:} + \sum_{i=i_1}^{i_r} \alpha_i^{(m,n)} \cdot \mathbf{X}_{i,:} + \mathbf{X}_{m,:} = \mathbf{0}. \quad (4)$$

In Eq. (4),  $i_1, \dots, i_r$  are the selected relay nodes, and  $\alpha_i^{(m,n)}$  is the corresponding coefficient that will be determined in advance (we will discuss this in Section III. D). As such,  $\mathbf{s}^*$  can be transmitted via the selected relay nodes  $i_1, \dots, i_r$ , each of which processes the received information via  $\alpha_i \cdot \mathbf{X}_{i,:}$ , and transmits the processed information to the next relay. Finally, Rx node  $m$  decrypts the received information via  $\mathbf{X}_{m,:}$  and derive the decrypted information  $\hat{\mathbf{s}}$ , i.e.,

$$\begin{aligned} \hat{\mathbf{s}} &= \mathbf{s}^* + \sum_{i=i_1}^{i_r} \alpha_i^{(m,n)} \cdot \mathbf{X}_{i,:} + \mathbf{X}_{m,:} \\ &= \mathbf{s} + \left( \mathbf{X}_{n,:} + \sum_{i=i_1}^{i_r} \alpha_i^{(m,n)} \cdot \mathbf{X}_{i,:} + \mathbf{X}_{m,:} \right) \\ &= \mathbf{s}. \end{aligned} \quad (5)$$

From Eqs. (3)-(5), it is seen that the essence of the proposed GLS is to use the channel-irrelevant networked dynamics on each node as the additive noise for security guarantees. Attributed to the dependencies of dynamics on different nodes, such additive noise can be compensated step-by-step by the corresponding relay nodes and the Rx node, whereby  $\boldsymbol{\alpha}^{(Tx,Rx)} = [\alpha_{i_1}^{(Tx,Rx)}, \dots, \alpha_{i_r}^{(Tx,Rx)}]^T$  accounts for the dependency coefficients. As such, to ensure the secure communication between any  $(Tx, Rx) \in \mathcal{N}^2$  node pair, each node  $i$  should save a dependency coefficient matrix of size  $N \times N$ , in which the  $(m, n)$ th element is  $\alpha_i^{(m,n)}$  representing its contribution to compensate the underlying dynamics of  $(Tx, Rx) = (m, n)$  pair. In the following, we will elaborate an off-line data-driven computation of the dependency coefficients, which avoids the use of the real-time networked dynamic for encryption, but is able to capture the networked dynamic dependency from the simulated training data.

#### A. GLS Secrecy Rate

The secrecy rate of the GLS encryption is the channel capacity subtraction between legitimate  $(Tx, Rx)$  pairs and the wiretap channels. Here, we consider a simplified passive eavesdropper for secrecy rate computation, where the eavesdropping can only happen by intercepting the transmitted/received signal at Tx or Rx. Other sophisticated attackers (e.g., an active attacker) are examined in Section III.C and in the simulations.

Given Eqs. (3)-(5), the legitimate channel capacity of the  $(Tx, Rx)$  communication node-pair can be expressed as:

$$C_{Tx,Rx} = \log_2 \left( 1 + \frac{\mathbb{E}(\mathbf{s})^2}{\|\mathbf{X}^T \cdot \boldsymbol{\alpha}^{(Tx,Rx)}\|_F^2 + \|\boldsymbol{\alpha}^{(Tx,Rx)}\|_2^2 \cdot \sigma^2} \right), \quad (6)$$

In Eq. (6),  $\mathbb{E}(\mathbf{s})$  accounts for the expectation of the information.  $\boldsymbol{\alpha}^{(Tx,Rx)} = [\alpha_1^{(Tx,Rx)}, \dots, \alpha_N^{(Tx,Rx)}]^T$  is the stacked weight

vector of Tx node, selected relays and Rx node, with zeros for unselected nodes.  $\|\mathbf{X}^T \cdot \boldsymbol{\alpha}^{(Tx,Rx)}\|_F^2$  (with the Frobenius norm  $\|\cdot\|_F$ ) therefore represents the residual energy after the process of Tx, selected relays and Rx.  $\|\boldsymbol{\alpha}^{(Tx,Rx)}\|_2^2 \cdot \sigma^2$  gives the weighted variance of the physical measuring noise induced by the dynamic extraction sensors, whose sampling noise is assumed to follow the Gaussian distribution with zero mean and variance as  $\sigma^2$ .

Similarly, the channel capacity from Tx to an eavesdropper that is proximate at Tx and Rx can be formulated as follows:

$$C_{\text{eav}}^j = \log_2 \left( 1 + \frac{\mathbb{E}(\mathbf{s})^2}{\|\boldsymbol{\alpha}_j^{(Tx,Rx)} \cdot \mathbf{X}_{j,:}\|_2^2} \right), \quad j \in \{Tx, Rx\}. \quad (7)$$

In Eq. (7), we remove the noise component to achieve an upper-bound eavesdropping channel capacity, which simplifies the following secrecy rate analysis for relay node selection and their weight computation.

With the help of the legitimate and wiretap channel capacities in Eqs. (6-7), the secrecy rate is specified as their difference:

$$R_{\text{Tx,Rx}} = \left[ C_{\text{Tx,Rx}} - \max_{j \in \{Tx, Rx\}} C_{\text{eav}}^j \right]^+, \quad (8)$$

where  $[x]^+ = \max(x, 0)$ . Then, we will elaborate how to select the relay nodes and their weights by maximizing the secrecy rate  $R_{\text{Tx,Rx}}$ , in the absence of the networked dynamics  $\mathbf{X}$ .

### B. Relay Selection & Weight Computation

To implement the GLS node pair encryption and communication in Eqs. (4)-(5), one require to select the appropriate relays and compute their weights. We do so by maximizing the secrecy rate  $R_{\text{Tx,Rx}}$  formulated in Eq. (8). To be specific, for each (Tx,Rx) communication pair, we compute the optimal weight vector  $\boldsymbol{\alpha}^{(Tx,Rx)} \in \mathbb{R}^N$  by solving the following optimization problem:

$$\begin{aligned} \max_{\boldsymbol{\alpha}^{(Tx,Rx)}} & \left[ \log_2 \left( 1 + \frac{\mathbb{E}(\mathbf{s})^2}{\|\mathbf{X}^T \cdot \boldsymbol{\alpha}^{(Tx,Rx)}\|_F^2 + \|\boldsymbol{\alpha}^{(Tx,Rx)}\|_2^2 \cdot \sigma^2} \right) \right. \\ & \left. - \max_{j \in \{Tx, Rx\}} \log_2 \left( 1 + \frac{\mathbb{E}(\mathbf{s})^2}{\|\boldsymbol{\alpha}_j^{(Tx,Rx)} \cdot \mathbf{X}_{j,:}\|_2^2} \right) \right]^+. \end{aligned} \quad (9)$$

As such, the relay selection is converted to the weight computation problem whereby the non-zero weights account for the selection of the corresponding nodes.

In Eq. (9), two challenges remain. First, the physical dynamic  $\mathbf{X}$  is unknown, which makes Eq. (9) difficult to be solved. Second, the objective function in Eq. (9) is non-concave (for maximization) with respect to  $\boldsymbol{\alpha}^{(Tx,Rx)}$ , although the feasible region is convex. To address the above challenges, we use a data-driven GFT operator as a surrogate matrix for  $\mathbf{X}$ , and then transform the non-concave maximization problem into an approximated convex optimization. We elaborate these two in the following.

1) *GFT Operator Based Surrogate*: Suppose that the physical networked dynamic matrix can be decomposed as  $\mathbf{X} = \mathbf{\Gamma} \cdot \tilde{\mathbf{X}}$  with  $\text{rank}(\mathbf{\Gamma}) = \text{rank}(\mathbf{X})$ . Then, if  $\mathbf{\Gamma}$  is only related with the dynamic model, and is therefore invariant with different initialization cases, such a  $\mathbf{\Gamma}$  can be used as the surrogate matrix for analyzing the row (node) dependency of  $\mathbf{X}$  in Eq. (9).

To implement this idea, we adopt the graph spectrum analysis and the concept of graph bandlimitedness from [20]–[25]. Before we start, we give a brief introduction of the graph Fourier transform (GFT) and the graph bandlimitedness. Given a GFT operator as  $\mathbf{U}^{-1}$  (typically an orthogonal matrix of size  $N \times N$ , i.e.,  $\mathbf{U}^{-1} = \mathbf{U}^T$ ), the processes of GFT and inverse GFT is specified as follows [20]–[26]:

$$\tilde{\mathbf{x}} = \mathbf{U}^{-1} \cdot \mathbf{x}, \quad (10)$$

$$\mathbf{x} = \mathbf{U} \cdot \tilde{\mathbf{x}}, \quad (11)$$

where  $\mathbf{x}$  of size  $N \times 1$  is the graph signal, and  $\tilde{\mathbf{x}}$  is its the graph frequency response. We call  $\mathbf{x}$  graph  $\mathcal{R}$ -bandlimited to the GFT operator  $\mathbf{U}^{-1}$ , if only the elements of  $\tilde{\mathbf{x}}$  with rows in the set  $\mathcal{R} \subset \{1, \dots, N\}$  are non-zeros.

According to the work in [19], this property holds for a vast variety of the time-varying networked dynamics in real-world systems, i.e., either the original  $\mathbf{X}_{:,k}$  or the time difference  $\mathbf{X}_{:,k} - \mathbf{X}_{:,k-1}$  are (or can be approximately treated as) graph  $\mathcal{R}$ -bandlimited to  $\mathbf{U}^{-1}$  for all time indices  $k$ . Here, we denote  $\mathbf{Y}$  as the original graph signal or the corresponding time difference, i.e.,

$$\mathbf{Y} = \begin{cases} \mathbf{X} & \mathbf{X}_{:,k} \text{ are graph bandlimited} \\ [\mathbf{X}_{:,k} - \mathbf{X}_{:,k-1}] & \text{with all } k \\ \mathbf{X}_{:,k} - \mathbf{X}_{:,k-1} & \text{are graph bandlimited} \end{cases} \quad (12)$$

where the selection is dependent on difference scenarios. As such, by denoting  $\mathbf{Y} = \mathbf{X}$  or  $[\mathbf{X}_{:,k} - \mathbf{X}_{:,k-1}]$  with all  $k$ , an surrogate of  $\mathbf{Y}$  can be assigned as  $\mathbf{\Gamma} = \mathbf{U}_{:, \mathcal{R}}$ , if  $\mathbf{Y}_{:,k}$  for all time indices  $k$  are graph  $\mathcal{R}$ -bandlimited to  $\mathbf{U}^{-1}$ , i.e.,

$$\mathbf{Y}_{:,k} = \mathbf{U}_{:, \mathcal{R}} \cdot \tilde{\mathbf{Y}}_{\mathcal{R},k}. \quad (13)$$

Here, for  $\mathbf{Y} = [\mathbf{X}_{:,k} - \mathbf{X}_{:,k-1}]$  with all  $k$ , we need to replace the original physical graph signal  $\mathbf{X}$  with the corresponding time difference  $\mathbf{Y}$ , in all GLS encryption and further processes, i.e., Eqs. (3)-(9).

In Eqs. (10)-(13), the GFT operator  $\mathbf{U}^{-1}$  is typically assigned as the eigenvector matrix of the graph adjacent matrix denoted as  $\mathbf{W}$  [20], [22], or the graph Laplacian matrix, computed as  $\mathbf{L} = \text{diag}(\mathbf{W} \cdot \mathbf{1}) - \mathbf{W}$  [23]–[25]. Accordingly, the graph bandlimited set  $\mathcal{R}$  is truncated from  $\{1, \dots, N\}$  to concentrate on the low graph bandlimited area (e.g., to minimize  $\mathbf{x}^T \cdot \mathbf{L} \cdot \mathbf{x}$  for Laplacian matrix). The problem here lies in the difficulty in measuring the actual elements in adjacent matrix  $\mathbf{W}$  (although with the known of the existence status of each link). To address this, we exploit a data-driven method, as we notice that the columns of  $\mathbf{U}_{:, \mathcal{R}}$  in Eq. (13) are the orthogonal vectors derived from the columns in  $\mathbf{Y}$ . As such we use  $D$  groups of training networked dynamics denoted

as  $\mathbf{Y}^{(d)}$ ,  $d = 1, \dots, D$ , and the GFT operator  $\mathbf{U}^{-1}$  can be computed as:

$$\begin{aligned} & \mathbf{U} \cdot \text{diag}([\lambda_1, \dots, \lambda_N]) \cdot \mathbf{U}^T \\ &= [\mathbf{Y}_{:,1:L}^{(1)}, \dots, \mathbf{Y}_{:,1:L}^{(D)}] \cdot [\mathbf{Y}_{:,1:L}^{(1)}, \dots, \mathbf{Y}_{:,1:L}^{(D)}]^T, \end{aligned} \quad (14)$$

where  $\lambda_1 > \dots > \lambda_N$  are the descended-ordered eigenvalues. Then, by measuring the maximal rank of all the training matrix, i.e.,  $r = \max_{d=1 \dots D} \text{rank}(\mathbf{Y}_{:,1:L}^{(d)})$ , we assign  $\mathcal{R} = \{1, \dots, r\}$ , and the surrogate matrix is computed as:

$$\mathbf{\Gamma} = \mathbf{U}_{:,1:r}. \quad (15)$$

Here, it is noteworthy that for any discrete-time  $k_i$  with a non-zero input perturbation  $\mathbf{b}_{k_i} \neq \mathbf{0}$ , the GFT based surrogate  $\mathbf{\Gamma}$  may not be able to characterize  $\mathbf{X}_{:,k} = \mathbf{\Gamma} \cdot \tilde{\mathbf{X}}_{:,k}$  or  $\mathbf{X}_{:,k} - \mathbf{X}_{:,k-1} = \mathbf{\Gamma} \cdot (\tilde{\mathbf{X}}_{:,k} - \tilde{\mathbf{X}}_{:,k-1})$ , since the random  $\mathbf{b}_{k_i}$  may not belong to the graph bandlimited subspace spanned by the orthogonal columns of  $\mathbf{\Gamma}$ . However, given that the injection perturbation is either sparse (e.g., the contaminant injection of the water-distribution network), or with small magnitudes (e.g., the power usage changes in the electrical bus system), this will not severely affect the dynamic dependency characterized by the graph bandlimited subspace for GLS encryption (we show this via Figs. 3-6).

2) *Weight Computation*: After the derivation of the physical networked dynamic surrogate in Eq. (15), we elaborate the process to approximate the non-concave maximization problem in Eq. (9) into a convex minimization form for optimal (sub-optimal) weight computation. By replacing the unknown networked dynamic matrix  $\mathbf{X}$  with the surrogate matrix  $\mathbf{\Gamma}$ , we re-write Eq. (9) as follows:

$$\begin{aligned} & \max_{\boldsymbol{\alpha}^{(Tx,Rx)}} \left[ \log_2 \left( 1 + \frac{\mathbb{E}(\mathbf{s})^2}{\|\mathbf{\Gamma}^T \cdot \boldsymbol{\alpha}^{(Tx,Rx)}\|_F^2 + \|\boldsymbol{\alpha}^{(Tx,Rx)}\|_2^2 \cdot \sigma^2} \right) \right. \\ & \quad \left. - \max_{j \in \{Tx, Rx\}} \log_2 \left( 1 + \frac{\mathbb{E}(\mathbf{s})^2}{\|\alpha_j^{(Tx,Rx)} \cdot \mathbf{\Gamma}_{j,:}\|_2^2} \right) \right]^+ \end{aligned} \quad (16)$$

We firstly remove the operator  $[\cdot]^+$ , and prove that the optimal value of Eq. (16) is same with that of the following form:

$$\begin{aligned} & \max_{\boldsymbol{\alpha}^{(Tx,Rx)}} \left[ \log_2 \left( 1 + \frac{\mathbb{E}(\mathbf{s})^2}{\|\mathbf{\Gamma}^T \cdot \boldsymbol{\alpha}^{(Tx,Rx)}\|_F^2 + \|\boldsymbol{\alpha}^{(Tx,Rx)}\|_2^2 \cdot \sigma^2} \right) \right. \\ & \quad \left. - \max_{j \in \{Tx, Rx\}} \log_2 \left( 1 + \frac{\mathbb{E}(\mathbf{s})^2}{\|\alpha_j^{(Tx,Rx)} \cdot \mathbf{\Gamma}_{j,:}\|_2^2} \right) \right]. \end{aligned} \quad (17)$$

Suppose  $L_1$  and  $L_2$  are the optimal values of Eq. (16) and Eq. (17) respectively. It is straightforward that  $L_1 \geq L_2$ , as Eq. (16) always takes the maximal value from Eq. (17) and 0. Then, denote  $\boldsymbol{\alpha}_*$  as the solution of Eq. (16) corresponding to the maximal value  $L_1 > 0$ . The value of Eq. (17) at  $\boldsymbol{\alpha}_*$  equaling  $L_1$ , suggests that the maximal value of Eq. (17), i.e.,  $L_2$ , is no less than  $L_1$ , i.e.,  $L_2 \geq L_1$ . This combined with aforementioned analysis of  $L_1 \geq L_2$ , proves that  $L_1 = L_2$ , which validates the replacement of original objective function in Eq. (16) with that of Eq. (17).

The problem then is converted to minimize the opposite of Eq. (17), i.e.,

$$\begin{aligned} & \min_{\boldsymbol{\alpha}^{(Tx,Rx)}} \left[ -\log_2 \left( 1 + \frac{\mathbb{E}(\mathbf{s})^2}{\|\mathbf{\Gamma}^T \cdot \boldsymbol{\alpha}^{(Tx,Rx)}\|_F^2 + \|\boldsymbol{\alpha}^{(Tx,Rx)}\|_2^2 \cdot \sigma^2} \right) \right. \\ & \quad \left. + \max_{j \in \{Tx, Rx\}} \log_2 \left( 1 + \frac{\mathbb{E}(\mathbf{s})^2}{\|\alpha_j^{(Tx,Rx)} \cdot \mathbf{\Gamma}_{j,:}\|_2^2} \right) \right]. \end{aligned} \quad (18)$$

In Eq. (18), it is seen that the second term is a convex function with respect to  $\alpha_j^{(Tx,Rx)}$ . We will then make the the first term of Eq. (18) convex, by introducing a slack variable  $\beta$ . The objective problem in Eq. (18) is converted as:

$$\begin{aligned} & \min_{\boldsymbol{\alpha}^{(Tx,Rx)} \atop \beta} \left[ -\log_2 \left( 1 + \frac{\mathbb{E}(\mathbf{s})^2}{\beta} \right) \right. \\ & \quad \left. + \max_{j \in \{Tx, Rx\}} \log_2 \left( 1 + \frac{\mathbb{E}(\mathbf{s})^2}{\|\alpha_j^{(Tx,Rx)} \cdot \mathbf{\Gamma}_{j,:}\|_2^2} \right) \right] \end{aligned} \quad (19a)$$

$$\text{s.t. } \|\mathbf{\Gamma}^T \cdot \boldsymbol{\alpha}^{(Tx,Rx)}\|_F^2 + \|\boldsymbol{\alpha}^{(Tx,Rx)}\|_2^2 \cdot \sigma^2 - \beta \leq 0. \quad (19b)$$

In Eq. (19a),  $\beta$  is assigned as an upper-estimator of  $\|\mathbf{\Gamma}^T \cdot \boldsymbol{\alpha}^{(Tx,Rx)}\|_F^2 + \|\boldsymbol{\alpha}^{(Tx,Rx)}\|_2^2 \cdot \sigma^2$ , therefore making the objective function in Eq. (19a) an upper-estimator of that in Eq. (18). As such, the minimization problem in Eq. (18) can be converted to minimizing its upper-estimator in Eq. (19a) with the constraint in Eq. (19b).

Then, it is noteworthy that  $-\log_2(1 + \mathbb{E}(\mathbf{s})^2/\beta)$  is a concave function with respect to  $\beta$ . To transform  $-\log_2(1 + \mathbb{E}(\mathbf{s})^2/\beta)$  as a convex form, we adopt the first-order Taylor expansion to represent the upper-estimator. As such, the minimization problem in Eq. (19) can be approximated by minimizing its convex upper-bound with the convex constraint. Accordingly, an iterative algorithm applying the successive convex optimization method can be designed. By assuming a given initial point as  $\beta_{\text{ini}}$  from last epoch, the first-order Taylor expansions of  $\log_2(1 + \mathbb{E}(\mathbf{s})^2/\beta)$  at  $\beta_{\text{ini}}$  is expressed respectively as:

$$\begin{aligned} -\log_2 \left( 1 + \frac{\mathbb{E}(\mathbf{s})^2}{\beta} \right) & \leq -\log_2 \left( 1 + \frac{\mathbb{E}(\mathbf{s})^2}{\beta_{\text{ini}}} \right) \\ & \quad + \frac{\mathbb{E}(\mathbf{s})^2 \cdot (\beta - \beta_{\text{ini}})}{\ln 2 \cdot (\beta_{\text{ini}}^2 + \mathbb{E}(\mathbf{s})^2 \cdot \beta_{\text{ini}})}, \end{aligned} \quad (20)$$

With the help of Eq. (20), we take it into Eq. (19), and add the  $l_1$ -norm of  $\boldsymbol{\alpha}^{(Tx,Rx)}$  to constrain the number of selected relays. The approximated convex optimization problem is obtained as follows:

$$\begin{aligned} & \min_{\boldsymbol{\alpha}^{(Tx,Rx)} \atop \beta} \left[ \frac{\mathbb{E}(\mathbf{s})^2 \cdot (\beta - \beta_{\text{ini}})}{\ln 2 \cdot (\beta_{\text{ini}}^2 + \mathbb{E}(\mathbf{s})^2 \cdot \beta_{\text{ini}})} \right. \\ & \quad \left. + \max_{j \in \{Tx, Rx\}} \log_2 \left( 1 + \frac{\mathbb{E}(\mathbf{s})^2}{\|\alpha_j^{(Tx,Rx)} \cdot \mathbf{\Gamma}_{j,:}\|_2^2} \right) + \|\boldsymbol{\alpha}^{(Tx,Rx)}\|_1 \right] \end{aligned} \quad (21a)$$

$$\text{s.t. } \|\mathbf{\Gamma}^T \cdot \boldsymbol{\alpha}^{(Tx,Rx)}\|_F^2 + \|\boldsymbol{\alpha}^{(Tx,Rx)}\|_2^2 \cdot \sigma^2 - \beta \leq 0. \quad (21b)$$

---

**Algorithm 1** Offline Relay Selection Algorithm
 

---

**Input:**  $D$  groups of training data, i.e.,  $\mathbf{Y}$  of networked dynamics.

- 1: Compute GFT based dynamic surrogate using Eqs. (14)-(15).
- 2: Assign  $k = 0$ . Find an initial feasible solution  $\alpha^{(\text{Tx,Rx})}(0)$  and an initial slack variable  $\beta(0)$ . Assign  $\Delta(0) = f(\alpha^{(\text{Tx,Rx})}(0))$ .
- 3: **while**  $\Delta(k) > \epsilon$  **do**
- 4:   Assign  $k = k + 1$ .
- 5:   Update  $\alpha^{(\text{Tx,Rx})}(k)$  and  $\beta(k)$  by solving convex problem in Eq. (21) with initial variables  $\alpha^{(\text{Tx,Rx})}(k-1)$  and  $\beta(k-1)$ .
- 6:   Compute  $\Delta(k) = f(\alpha^{(\text{Tx,Rx})}(k)) - f(\alpha^{(\text{Tx,Rx})}(k-1))$ .
- 7: **end while**
- 8: Assign  $\alpha^{(\text{Tx,Rx})}(k)$  as optimal  $\alpha^{(\text{Tx,Rx})}$ .

**Output:** Return  $\alpha^{(\text{Tx,Rx})}$ .

---

3) *Overall Relay Selection Algorithm:* After the elaborate of the GFT based surrogate and the weight computation, we provide the relay selection algorithm in Algorithm 1. The input is the training data of the physical networked dynamic for GFT surrogate  $\Gamma$  computation. Step 1 is to compute the GFT surrogate that will be used for following weight computation. Step 2 is the initialization for the successive convex optimization method of weight computation. Steps 3-7 is to pursue the successive convex optimization, in which the weight vector  $\alpha^{(\text{Tx,Rx})}$  is successively computed by solving the convex problem in Eq. (21). Then, the output is the computed weight  $\alpha^{(\text{Tx,Rx})}$ .

It is noteworthy that the proposed relay selection algorithm is in the offline manner. To be specific, the relay is selected without any knowledge of the real networked dynamics that will be used for communication encryption, but the dynamic training data from the simulator that is able to characterize the dependencies of the physical networked dynamics. In this view, two benefits are given in the following. First, the relays and their weights can be computed and saved in advance, and do not need to be re-evaluated if the hidden governing dynamic equations in Eq. (1) and the network topology are fixed. As such, the computational complexity of the relay selection algorithm is trivial, and no delay will be caused by the algorithm in the securing of wireless communications. Second, the computations of the relays and their weights do not depend on the real networked dynamics that will be used for information encryption, which suggests the communication security even if the selected relays and their weights are revealed by an active or a passive attacker. We will discuss this in the following parts.

### C. Active & Passive Attackers

After the elaboration of the GLS encryption, we discuss two types of the eavesdroppers, i.e., the passive and active attackers.

1) *Passive Eavesdropper:* In the context of GLS where the physical networked dynamic is used for encryption, a

passive eavesdropper is defined to intercept the transmitted information without degrading the physical networked dynamics. In this view, the eavesdropper can 1) intercept only the transmitted information, or 2) in a more sophisticated way, equip eavesdropping sensors on parts of the network nodes and try to recover the whole physical networked dynamic matrix  $\mathbf{X}$ . The former has been discussed in Eq. (9), i.e., the eavesdropper can be intercepted the transmitted information at Tx or Rx, and the further optimal relay selection and weight computation in Eq. (21) can ensure the maximal secrecy rate. We will show the GLS performance with the eavesdropper that only intercept the transmitted information in Figs. 3-4.

For the latter, the GLS encryption performance will be degraded in terms of how accurate the eavesdropper recovers the unknown physical networked dynamic  $\mathbf{X}$ , and this depends on how many network nodes have been hacked by the eavesdropping sensors. Here, we analyze the worst case in which the eavesdropper knows the data-driven GFT surrogate  $\Gamma$ , and the weight vector  $\alpha^{(\text{Tx,Rx})}$  for each (Tx, Rx) pair, and can use smallest number of network nodes to recover  $\mathbf{X}$ . According to the graph sampling theory [20]–[25], the full recovery of  $\mathbf{X}$  is guaranteed when eavesdropper equips sensors on the subset of all network nodes  $\mathcal{S} \subset \{1, \dots, N\}$  such that

$$\text{rank}(\Gamma_{\mathcal{S},:}) = r. \quad (22)$$

Eq. (22) is implemented via a *greedy* algorithm that minimizes the condition number of  $\Gamma_{\mathcal{S},:}$  by finding and adding row index to  $\mathcal{S}$ , i.e.,  $\mathcal{S} \leftarrow \mathcal{S} \cup \{i\}$ , such that  $i = \text{argmin}_{j \in \mathcal{N} \setminus \mathcal{S}} \text{cond}(\Gamma_{\mathcal{S}+\{j\},:})$ . After eavesdropping the physical networked dynamics from nodes corresponding to  $\mathcal{S}$  as  $\mathbf{X}_{\mathcal{S},:}$ , the eavesdropper can recover the complete networked dynamics as [20]–[25]:

$$\hat{\mathbf{X}} = \Gamma_{:,1:r} \cdot \Gamma_{\mathcal{S},1:r}^\dagger \cdot \mathbf{X}_{\mathcal{S},:}, \quad (23)$$

which will then be used for decrypting the intercepted information.

It is noteworthy that hacking different network nodes for physical networked dynamic recovery is a strong assumption for eavesdroppers, as they have to know the data-driven GFT surrogate  $\Gamma$ , and the weight vector  $\alpha^{(\text{Tx,Rx})}$  for each (Tx, Rx) pair, not to mention how difficult to embed eavesdropping sensors on a number of network nodes without being detected. We will show the number of nodes being hacked versus the GLS performance in Figs. 3-4 in the simulation part.

2) *Active Attackers:* The active attacker in GLS is defined to degrade the networked dynamics and their dependencies, which will subsequently deteriorate the GLS encryption that relies on them. The method is to frequently inject a harmful jamming input to the networked dynamical system. Here, different from perturbation  $\mathbf{b}_k$  in Eq. (1), the jamming injection is more frequent and with larger amplitudes. For example, in the electric bus system, an active attacker can steeply add a huge and harmful power usages at a single or multiple buses, and subsequently affects the whole networked dynamic (such as rotor speed and angle).

In this view, the GLS performance depends on whether the GFT based surrogate matrix  $\Gamma$  is still holding for analyzing the linearly dependency of rows (i.e., relay selection and weight

computation) in  $\mathbf{X}$ . It is straightforward that an increasing rate of jamming injection will make  $\mathbf{\Gamma}$  fail to represent  $\mathbf{X} = \mathbf{\Gamma}\mathbf{\tilde{X}}$ , as a large perturbation can be artificially designed by orthogonal vectors that do not belong to the graph bandlimited subspace spanned by the columns of  $\mathbf{\Gamma}$ . We will evaluate the GLS performance versus the active attackers with different injection rates in Fig. 5-6 in the simulation part.

#### IV. SIMULATIONS AND RESULTS

##### A. Experimental Setting

The underlying network and the physical dynamics are configured as the IEEE 39-Bus system [27]–[29]. The network is with  $N = 39$  nodes (10 generator buses  $i = 30, \dots, 39$  and 29 load buses  $i = 1, \dots, 29$ ), as is shown by Fig. 2. The physical dynamic model over the network are expressed by following differential and algebraic equations (DAEs) [27], [30]:

$$\frac{d\theta_i(t)}{dt} = \Delta\omega_i(t) \quad i \in \{1, \dots, 39\} \quad (24)$$

$$\frac{d\Delta\omega_i(t)}{dt} = \frac{\omega_s}{2H_i} \cdot (T_i(t) - P_i(t) - D \cdot \Delta\omega_i(t)) \quad i \in \{30, \dots, 39\} \quad (25)$$

$$T_i(t) = - \left( K_P \cdot \Delta\omega_i(t) + K_I \int_0^t \Delta\omega_i(\tau) d\tau \right) \quad i \in \{30, \dots, 39\} \quad (26)$$

$$P_i(t) = \sum_{j=1}^{39} G_{i,j} \cos(\theta_i(t) - \theta_j(t)) + B_{i,j} \sin(\theta_i(t) - \theta_j(t)) \quad i \in \{30, \dots, 39\} \quad (27)$$

$$PL_i = \sum_{j=1}^{39} G_{i,j} \cos(\theta_i(t) - \theta_j(t)) + B_{i,j} \sin(\theta_i(t) - \theta_j(t)) \quad i \in \{1, \dots, 29\}. \quad (28)$$

In Eqs. (24)–(28),  $\theta_i(t)$  is the phasor's angle at  $i$  bus, and  $\Delta\omega_i(t)$  is the phasor's speed deviation (i.e., the difference between actual speed and the nominal synchronous speed  $\omega_s = 2\pi \cdot 60 \text{ rad/s}$ ). For generator node  $i$  (i.e.,  $i = 30, \dots, 39$ ),  $H_i$  is the inertia constant,  $T_i(t)$  is the mechanical torque controlling the generator's speed deviation (with constants  $K_I$  and  $K_P$ ), and  $P_i(t)$  is the electric air-gap torque affected by the neighbour nodes' angles.  $G_{i,j}$  and  $B_{i,j}$  are respectively the real and imaginary parts of the  $(i, j)$ th element of admittance matrix, which characterizes the admittance of power lines between buses. The aforementioned parameters are assigned according to the work in [27]. In Eq. (28),  $PL_i$  represents the load under bus  $i$ , following a Gaussian distribution with empirical expectation and variance, which accounts for the dynamical input of the system that affects the networked dynamics (i.e., the angles and the speed deviation). We also emphasize here, that the aforementioned DAEs are only used for physical dynamic generation, and are unknown for the encryption and communication processes (e.g. process is data driven and model agnostic).

With the help of the dynamic model, we select the speed deviation as the physical networked signal for GLS encryption.

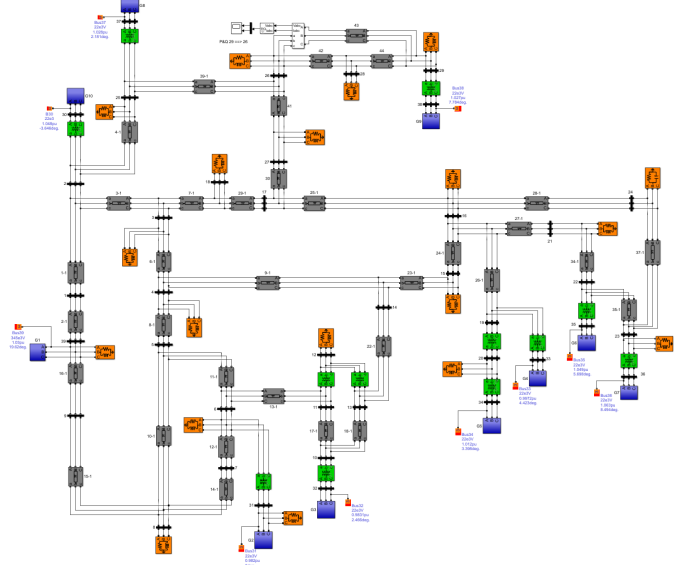


Fig. 2. Network topology of IEEE 39-Bus system, with  $N = 39$  buses (nodes) including 10 generators (buses 30-39) and 29 load buses (1-29).

To be specific, each bus (node)  $i$  is equipped with an IoT sensor (e.g., the phasor measurement unit PMU), aiming at measuring the speed deviation from time  $t = 0$  to  $t = 5$ , by sampling rate  $T_s = 10^{-3} \text{ s}$  [31] (i.e., discrete-time  $K = 5000$ ). As such, the  $(i, k)$ th element of matrix  $\mathbf{X}$  in Eq. (1), is assigned as the measured  $\Delta\omega_i(t = k \cdot T_s)$ , with a **physical measurement noise** (not to be confused with communication SNR), which is used to encrypt (for Tx), process (for relays) and decrypt (for Rx) the transmitted information. In this simulation, any pair of nodes are tested as a transmitter (Tx), and a receiver (Rx). The information are assigned as the discrete on-off keying (OOK) with length  $K = 5000$ . The channels for such communications are wireless and are independent with the physical networked dynamics. For attackers, we test the aforementioned passive and active types respectively.

##### B. GLS Performance with Passive Eavesdroppers

We at first evaluate the GLS performance with passive eavesdroppers mentioned in Section III. E 1). For this experiment, four passive eavesdroppers are considered. The first one only intercepts the transmitted information without hacking any network node for the physical networked dynamics. The second to the fourth are considered to hack 5%, 10%, 25% network nodes and their underlying physical networked dynamics to recover the whole dynamic matrix  $\mathbf{X}$ , via the graph sampling theory in Eq. (22). Here, it is noteworthy that, the hacked node set  $\mathcal{S}$  are not randomly selected, but follows Eq. (22), i.e., satisfying  $\text{rank}(\mathbf{\Gamma}_{\mathcal{S},:}) = r$ . For example, in IEEE 39-Bus system,  $|\mathcal{S}| = 10$  (or  $|\mathcal{S}|/39 \approx 25\%$ ) selected by the graph sampling theory is  $\mathcal{S} = \{1, 2, 6, 10, 20, 21, 23, 25, 28, 33\}$ .

In Fig. 3(a), we provide the average BERs of legitimate (Tx,Rx) pairs and of eavesdroppers, versus the measurement noise variance (i.e.,  $\sigma^2$ ) of sensors for physical networked dynamic extraction. We can firstly observe that the BER of the legitimate users becomes lower (e.g.,  $10^{-1}$  to  $10^{-5}$ ) as



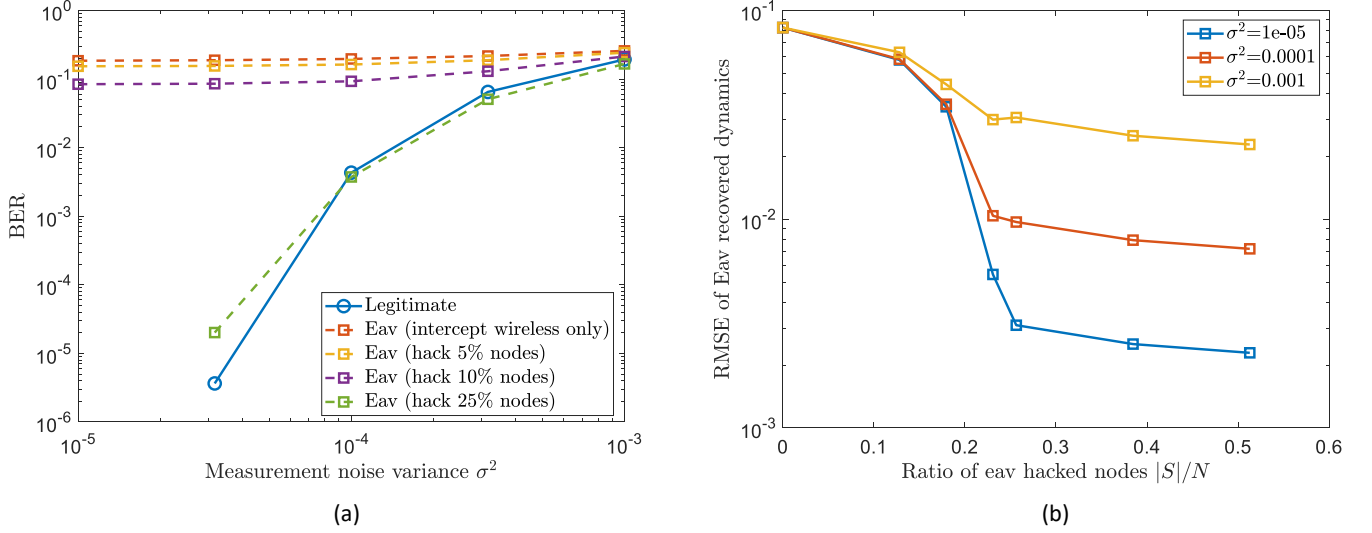


Fig. 3. GLS performance with Passive eavesdroppers: (a) Average BER with eavesdroppers hacking 0% nodes, 5% nodes, 10% nodes and 25% nodes. (b) Recovery RMSEs of physical dynamics by eavesdroppers hacking 0% nodes, 5% nodes, 10% nodes and 25% nodes.

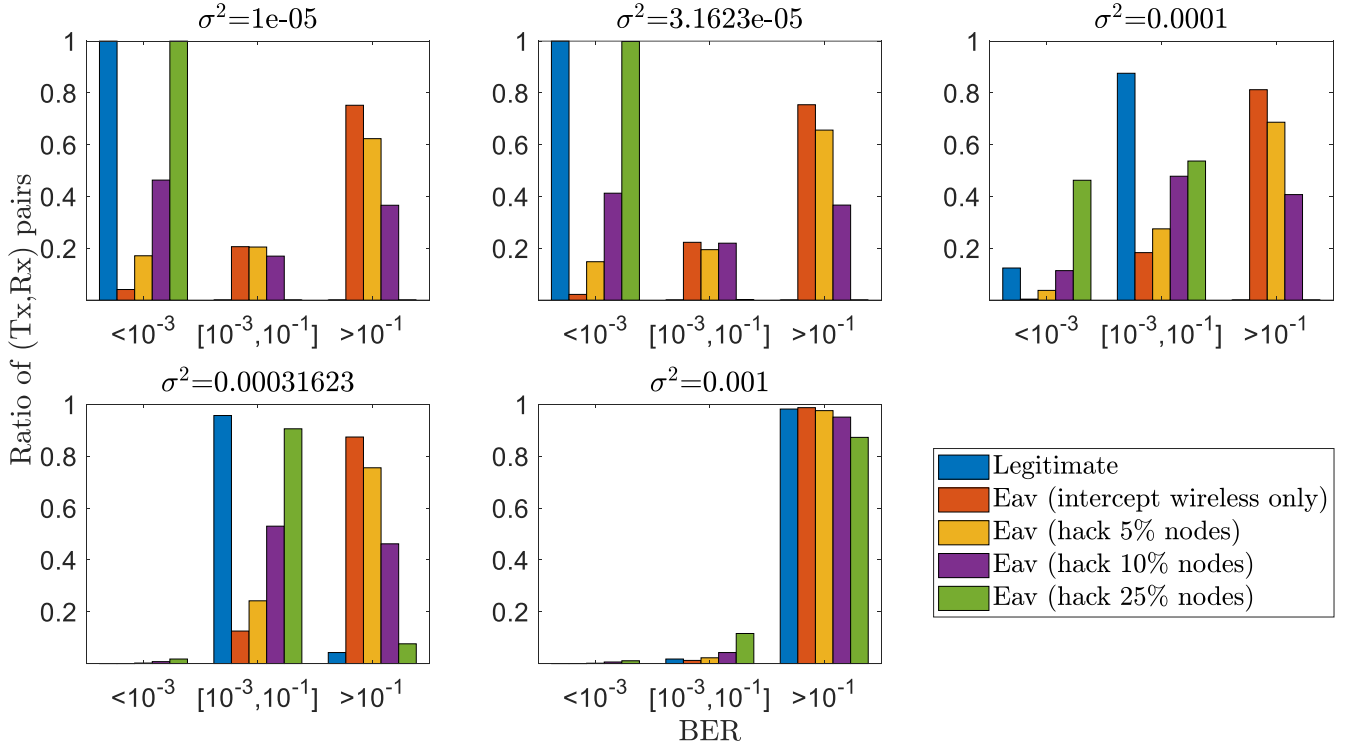


Fig. 4. Statistical distribution of all (Tx,Rx) pairs with respect to different levels of BERs.

$\sigma^2$  decreases (from  $10^{-3}$  to  $10^{-5}$ ). This highlights the security's dependency on sensor accuracy (i.e., physical measuring accuracy) rather than the wireless channel estimation quality or diversity (PLS) or public key security. For sensitive noise variance (as one expects of good IoT systems), the encrypted communication channel can achieve a decryption BER of  $\approx 10^{-5}$ , 5 orders of magnitude better than the eavesdroppers (that only intercept the wireless transmitted information). This indicates the encryption reliability of GLS, which can be ensured solely by a cheap but accurate physical sensors

(to extract and exploit the physical networked dynamics for communication security), as opposed to the existing wireless-based encryption (PLS) that requires complex and unreliable channel estimation techniques.

Then, it is seen that with the increase of nodes being hacked by the eavesdroppers, the eavesdropping BERs decrease. To be specific, the BER of eavesdroppers hacking 0% nodes (i.e., only intercept transmitted information) is higher than that hacking 5% nodes, higher than that hacking 10%, and the one with 25% hacked nodes are the lowest. This is analyzed with



the help of Fig. 3(b), where the dynamic recovery RMSEs by eavesdroppers versus the ratios of their hacked nodes are given, and that when the number of hacked nodes is larger than 25%, the RMSE converges. This is due to the graph sampling theory in Eq. (22), which indicates the appropriate node selection satisfying  $|\mathcal{S}| = r = 10$  can guarantee the complete dynamic recovery ( $r = 10$  here is given by the data characteristic of IEEE 39-Bus with 10 generators). As such, Fig. 3(b) gives the reason that eavesdroppers with  $10/39 \approx 25\%$  hacked nodes can obtain the whole underlying dynamic for encryption and therefore achieve successful decryption. However, it is noteworthy that hacking such a large number of nodes is difficult for the eavesdroppers, as they have to equip their eavesdropping sensors on every network node they are interested without being discovered. As such, our GLS method provides a novel perspective and security performance for IoT system, by the utilization of underlying physical networked dynamics that are hard to be extracted by the eavesdroppers.

In Fig. 4, we provide the statistical distribution of (Tx,Rx) pairs with respect to different BER regions, i.e.,  $< 10^{-3}$ , between  $10^{-3}$  and  $10^{-1}$ , and  $> 10^{-1}$ . It is seen that the ratios of (Tx,Rx) pairs belonging to the low BER regions are always larger than those from the passive eavesdroppers (except for the one hacking 25% network nodes and obtaining the full physical networked dynamics). For instance, when measurement noise variance  $\sigma^2 < 10^{-4}$ , the ratio of (Tx,Rx) with BER less than  $10^{-3}$  approach to 1, larger then those eavesdroppers (i.e., with hacking 0%, 5%, and 10% nodes). This statistical result, combined with the previous average result in Fig. 4, demonstrates the encryption robustness and reliability of the proposed GLS to secure wireless communications, against potential passive eavesdroppers.

### C. GLS Performance with Active Attackers

We next evaluate the GLS performance against active attackers. As is described in Section III. C 2), the active attackers here aim to degrade the dynamic dependency among network nodes by adding artificial jamming inputs into the network. In the context of the IEEE 39-Bus system, the jamming inputs are the variations of the power usages at each bus, following the Gaussian distribution with means equaling the reference power usages at each bus, and variance as 5 per unit (larger than that of the dynamic perturbation), which will then affect the underlying dynamics (i.e., the rotor speed deviations) for information encryption and decryption. Four active attackers are considered, and assigned with different levels of jamming rates, i.e.,  $0s^{-1}$ ,  $10s^{-1}$ ,  $100s^{-1}$ ,  $200s^{-1}$ , and  $500s^{-1}$ .

In Fig. 5, we provide the average BERs of the legitimate (Tx,Rx) pairs versus the measurement noise variance (i.e.,  $\sigma^2$ ), under different levels of jamming attacks. It is firstly seen that the BERs for all levels of jamming rates become lower, as the decrease of the measurement noise variance  $\sigma^2$ . This indicates the GLS reliability that relies on the measuring accuracy of the physical networked dynamics for information encryption and decryption. Then, it is observed that with the increase of the jamming rates, the communication performance becomes worse. For example, at the point  $\sigma^2 = 3.16 \times 10^{-5}$ , the BER

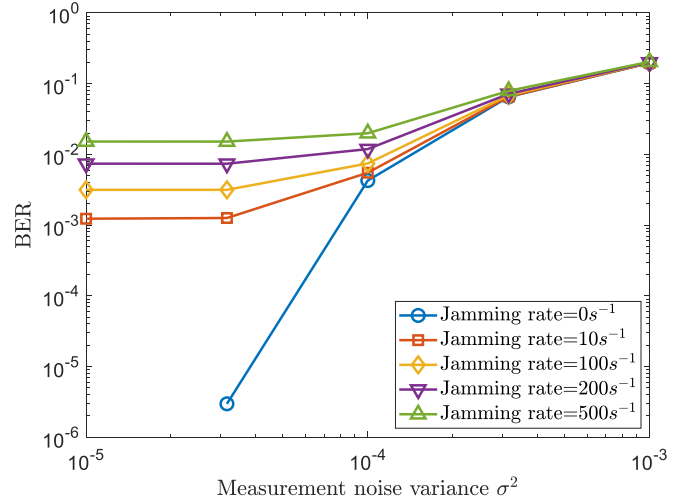


Fig. 5. GLS performance with active attackers: average BER versus physical measurement noise with different levels of jamming rate.

increases from an order of  $10^{-5}$  to  $10^{-2}$  when jamming rate increases from  $0s^{-1}$  to  $500s^{-1}$ . This is because (i) the burst jamming injection degrades the linear dependant property of the dynamics among the (Tx, relays, Rx) nodes, and (ii) with such increases of the jamming inputs deteriorate the successful decryption rate at Rx.

In Fig. 6, we provide the statistical distribution of (Tx,Rx) pairs with respect to different BER regions, i.e.,  $< 10^{-3}$ , between  $10^{-3}$  and  $10^{-1}$ , and  $> 10^{-1}$ , under different levels of the jamming rate from the active attackers. It is seen that, given the fixed physical measurement noise variance, with the increases of the attacker's jamming rate, the ratio of (Tx,Rx) pairs belonging to the low BER regions decreases. For instance, when measurement noise variance has an order as  $\sigma^2 = 10^{-5}$ , the ratio of (Tx,Rx) with no jamming belonging to  $BER < 10^{-3}$  approach to 1, larger then those affected by jamming input (i.e., with jamming rate  $10s^{-1}$ ,  $100s^{-1}$ ,  $200s^{-1}$  and  $500s^{-1}$ ). Nevertheless, with medium jamming rates and sensitive physical measurement noise regions as is depicted in Fig. 6 (i.e., jamming rate  $\leq 100s^{-1}$  and  $\sigma^2 \leq 10^{-4}$ ), the proposed GLS can still approach the 7 overhead hard-decision FEC limit (i.e.,  $BER \approx 4.5 \times 10^{-3}$ ) [32], indicating an error-free BER performance with proper FEC codes. This statistical result, combined with the previous average result in Fig. 5, demonstrates the encryption robustness and reliability of the proposed GLS to secure wireless communications, against potential active attackers.

## V. CONCLUSION

Graph Layer Security (GLS) is proposed for the first time here, as a way to secure the wireless communication information via the wireless channel -irrelevant networked domain physical dynamics. Our approach is premised on the exploration of the dependencies of nonlinear physical networked dynamics among the network nodes for encryption and decryption. The advantage of this approach, as described and demonstrated, is to rely solely on the IoT sensors' accuracy

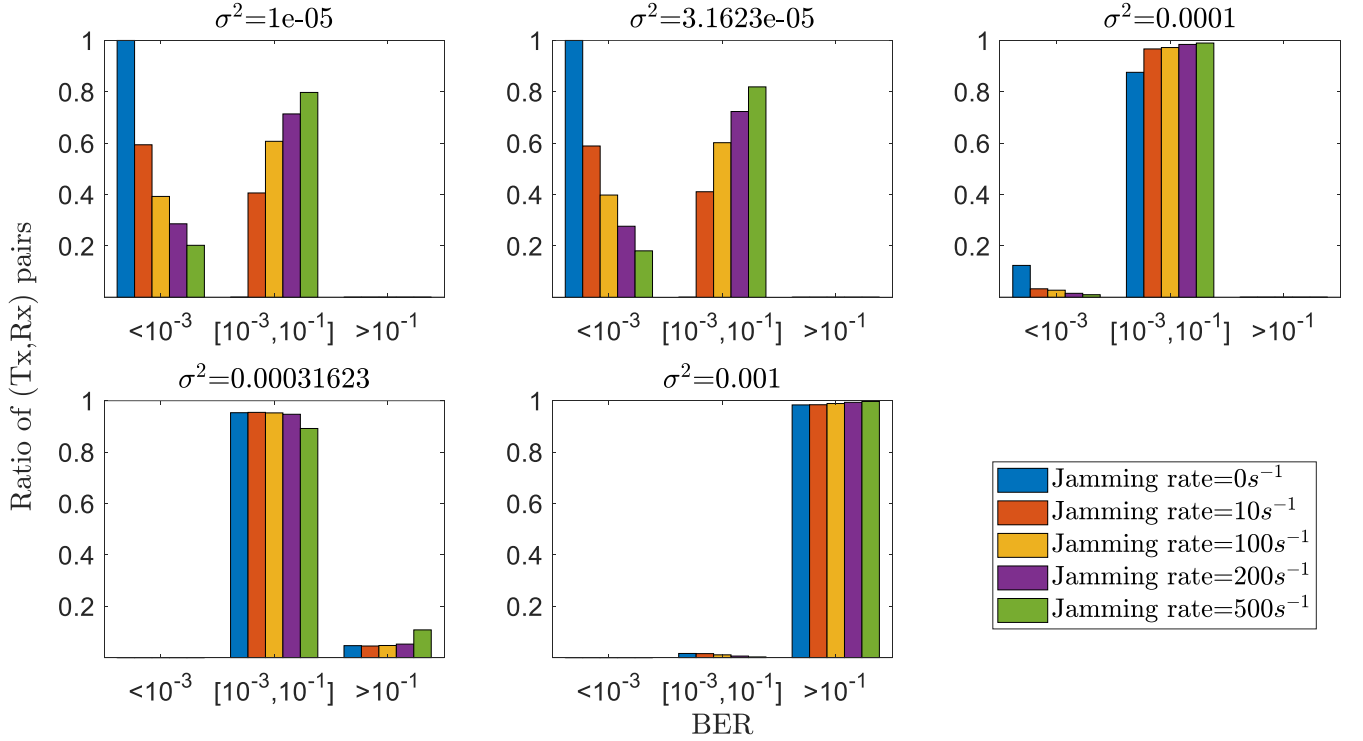


Fig. 6. GLS performance with active attackers: (a) Legitimate BER versus measurement noise No jamming, 5% nodes, 10% nodes and 25% nodes. (b) Recovery RMSEs of physical dynamics by eavesdroppers hacking 0% nodes, 5% nodes, 10% nodes and 25% nodes.

in measuring the physical dynamics  $\mathbf{X}$  (e.g. water flow rate, contamination, gas pressure, voltage) of a networked system. Over the past few decades, we have developed cheap and accurate sensors. Therefore, encrypting the wireless information by exploiting this accuracy makes sense compared to continuously and accurately estimating the wireless environment in PLS, which remains challenging for small IoT devices.

The challenge with GLS is to develop representative GFT operators that can characterize the dynamic dependency into a feasible graph bandlimited subspace, so that the (Tx,Rx) communication node pair can use such dependent channel-irrelevant dynamic to encrypt their transmitted information. This is especially hard for those that involve PDEs. Our prior work in sparse sensing of water distribution networks has shown that GSP can be applied successfully to Navier-Stokes PDEs in water distribution networks [4]. The generality of this data-driven approach is strong as it does not require knowledge of the underlying physical dynamic model, and indeed many real world systems do not have one or involve couplings between ODEs and PDEs (e.g. electricity grid connected to a thermo energy storage).

Then, leveraging the GFT operator, encryption and decryption schemes were designed by maximizing the GLS secrecy rate. The simulation results demonstrate the both the robustness and the reliability of the proposed GLS combating both the passive eavesdroppers and the active attackers, which suggests its widespread applicability in secure wireless communications over IoT systems, especially for the challenging radio environments and computational resource scarcity scenarios where traditional cryptography and PLS are less attractive.

Here, one problem lies in the relay mechanism in our GLS method, which may cause delay for information transmission and may increase the rate of interception by more sophisticated eavesdroppers. The reason lies in the exploitation of solely the linear dynamic dependency. In our future work, we will study how to extract and utilize the higher order dynamic dependency for point-to-point wireless communications over IoT systems.

## REFERENCES

- [1] B. Ahlgren, M. Hidell, and E. C. . Ngai, "Internet of things for smart cities: Interoperability and open data," *IEEE Internet Computing*, vol. 20, no. 6, pp. 52–56, 2016.
- [2] L. Wang and R. Ranjan, "Processing distributed internet of things data in clouds," *IEEE Cloud Computing*, vol. 2, no. 1, pp. 76–80, 2015.
- [3] N. Saeed, M. Alouini, and T. Y. Al-Naffouri, "Toward the internet of underground things: A systematic survey," *IEEE Communications Surveys Tutorials*, vol. 21, no. 4, pp. 3443–3466, 2019.
- [4] Z. Wei, A. Pagani, G. Fu, I. Guymer, W. Chen, J. McCann, and W. Guo, "Optimal sampling of water distribution network dynamics using graph fourier transform," *IEEE Transactions on Network Science and Engineering*, vol. 7, no. 3, pp. 1570–1582, Sep. 2020.
- [5] W. Ayoub, A. E. Samhat, F. Nouvel, M. Mroue, and J. Prévotet, "Internet of mobile things: Overview of lorawan, dash7, and nb-iot in lpwans standards and supported mobility," *IEEE Communications Surveys Tutorials*, vol. 21, no. 2, pp. 1561–1581, 2019.
- [6] H. V. Poor and R. F. Schaefer, "Wireless physical layer security," *Proceedings of the National Academy of Sciences*, vol. 114, no. 1, pp. 19–26, 2017.
- [7] A. Mukherjee, S. A. A. Fakoorian, J. Huang, and A. L. Swindlehurst, "Principles of physical layer security in multiuser wireless networks: A survey," *IEEE Communications Surveys Tutorials*, vol. 16, no. 3, pp. 1550–1573, Third Quarter 2014.
- [8] H. Wang, X. Zhang, and J. Jiang, "Uav-involved wireless physical-layer secure communications: Overview and research directions," *IEEE Wireless Communications*, vol. 26, no. 5, pp. 32–39, Oct. 2019.

- [9] X. Sun, D. W. K. Ng, Z. Ding, Y. Xu, and Z. Zhong, "Physical layer security in uav systems: Challenges and opportunities," *IEEE Wireless Communications*, vol. 26, no. 5, pp. 40–47, Oct. 2019.
- [10] G. Zhang, Q. Wu, M. Cui, and R. Zhang, "Securing uav communications via joint trajectory and power control," *IEEE Transactions on Wireless Communications*, vol. 18, no. 2, pp. 1376–1389, Feb. 2019.
- [11] X. Fang, N. Zhang, S. Zhang, D. Chen, X. Sha, and X. Shen, "On physical layer security: Weighted fractional fourier transform based user cooperation," *IEEE Transactions on Wireless Communications*, vol. 16, no. 8, pp. 5498–5510, Aug. 2017.
- [12] S. Rothe, N. Koukourakis, H. Radner, A. Lonnstrom, E. Jorswieck, and J. Czarske, "Physical layer security in multimode fiber optical networks," *Scientific Reports*, vol. 10, p. 2740, 2020.
- [13] B. Li, Z. Fei, Y. Zhang, and M. Guizani, "Secure uav communication networks over 5g," *IEEE Wireless Communications*, vol. 26, no. 5, pp. 114–120, Oct. 2019.
- [14] Y. Zhu, G. Zheng, and M. Fitch, "Secrecy rate analysis of uav-enabled mmwave networks using matérn hardcore point processes," *IEEE Journal on Selected Areas in Communications*, vol. 36, no. 7, pp. 1397–1409, Jul. 2018.
- [15] Y. Ai, M. Cheffena, A. Mathur, and H. Lei, "On physical layer security of double rayleigh fading channels for vehicular communications," *IEEE Wireless Communications Letters*, vol. 7, no. 6, pp. 1038–1041, Aug. 2018.
- [16] S. Hong, C. Pan, H. Ren, K. Wang, and A. Nallanathan, "Artificial-noise-aided secure mimo wireless communications via intelligent reflecting surface," *IEEE Transactions on Communications*, vol. 68, no. 12, pp. 7851–7866, Dec. 2020.
- [17] Y. Zhou, P. L. Yeoh, H. Chen, Y. Li, R. Schober, L. Zhuo, and B. Vucetic, "Improving physical layer security via a uav friendly jammer for unknown eavesdropper location," *IEEE Transactions on Vehicular Technology*, vol. 67, no. 11, pp. 11 280–11 284, Nov. 2018.
- [18] J. Zhang, S. Rejendran, Z. Sun, R. Woods, and L. Hanzo, "Physical layer security for the internet of things: Authentication and key generation," *IEEE Wireless Communications*, vol. 5, 2019.
- [19] K. Qiu, X. Mao, X. Shen, X. Wang, T. Li, and Y. Gu, "Time-varying graph signal reconstruction," *IEEE Journal of Selected Topics in Signal Processing*, vol. 11, no. 6, pp. 870–883, Jul. 2017.
- [20] S. Chen, R. Varma, A. Sandryhaila, and J. Kovacevic, "Discrete signal processing on graphs: Sampling theory," *IEEE Trans. Signal Process.*, vol. 63, no. 24, pp. 6510–6523, Dec. 2015.
- [21] A. Anis, A. Gadde, and A. Ortega, "Efficient sampling set selection for bandlimited graph signals using graph spectral proxies," *IEEE Trans. Signal Process.*, vol. 64, no. 14, pp. 3775–3789, Jul. 2016.
- [22] S. Chen, R. Varma, A. Singh, and J. Kovacevic, "Signal recovery on graphs: Fundamental limits of sampling strategies," *IEEE Trans. Signal Inf. Process. over Networks*, vol. 2, no. 4, pp. 539–554, Dec. 2016.
- [23] A. Ortega, P. Frossard, J. Kovacevic, J. M. F. Moura, and P. Vandergheynst, "Graph signal processing: Overview, challenges, and applications," *Proc. IEEE*, vol. 106, no. 5, pp. 808–828, May 2018.
- [24] D. Romero, V. N. Ioannidis, and G. B. Giannakis, "Kernel-based reconstruction of space-time functions on dynamic graphs," *IEEE Journal of Selected Topics in Signal Processing*, vol. 11, no. 6, pp. 856–869, 2017.
- [25] M. Tsitsvero, S. Barbarossa, and P. Di Lorenzo, "Signals on graphs: Uncertainty principle and sampling," *IEEE Transactions on Signal Processing*, vol. 64, no. 18, pp. 4845–4860, 2016.
- [26] Z. Wei, B. Li, C. Sun, and W. Guo, "Sampling and inference of networked dynamics using log-koopman nonlinear graph fourier transform," *IEEE Transactions on Signal Processing*, vol. 68, pp. 6187–6197, 2020.
- [27] P. W. Sauer and M. A. Pai, *Power system dynamics and stability*. Wiley Online Library, 1998, vol. 101.
- [28] X. Wang, J. Zhao, V. Terzija, and S. Wang, "Fast robust power system dynamic state estimation using model transformation," *International Journal of Electrical Power & Energy Systems*, vol. 114, p. 105390, 2020.
- [29] E. Ghahremani and I. Kamwa, "Local and wide-area pmu-based decentralized dynamic state estimation in multi-machine power systems," *IEEE Transactions on Power Systems*, vol. 31, no. 1, pp. 547–562, Jan. 2016.
- [30] J. Qi, K. Sun, and W. Kang, "Optimal pmu placement for power system dynamic state estimation by using empirical observability gramian," *IEEE Transactions on Power Systems*, vol. 30, no. 4, pp. 2041–2054, Jul. 2015.
- [31] Z. Wei, B. Li, and W. Guo, "Optimal sampling for dynamic complex networks with graph-bandlimited initialization," *IEEE Access*, vol. 7, pp. 150 294–150 305, 2019.
- [32] F. Chang, K. Onohara, and T. Mizuochi, "Forward error correction for 100 g transport networks," *IEEE Communications Magazine*, vol. 48, no. 3, pp. S48–S55, 2010.